Optical properties of Cu-chalcogenide photovoltaic absorbers from self-consistent GW and the Bethe-Salpeter equation

Sabine Körbel, David Kammerlander, Rafael Sarmiento-Pérez, Claudio Attaccalite, Miguel Alexandre Lopes Marques, Silvana Botti

Optical properties of Cu-chalcogenide photovoltaic absorbers from self-consistent *GW* and the Bethe-Salpeter equation

Sabine Körbel,[1,*] David Kammerlander,[1,2] Rafael Sarmiento-Pérez,[1,3] Claudio Attaccalite,[2,4] Miguel A. L. Marques,[1,4,5] and Silvana Botti[1,3,4,†]

[1]*Institut Lumière Matière, UMR5306 CNRS, Université Claude Bernard Lyon 1, F-69622 Villeurbanne Cedex, France*

[2]*Institut Néel, Université Joseph Fourier and CNRS, 38042 Grenoble Cedex 9, France*

[3]*Institut für Festkörpertheorie und -optik, Friedrich-Schiller-Universität Jena, Max-Wien-Platz 1, 07743 Jena, Germany*

[4]*European Theoretical Spectroscopy Facility*

[5]*Institut für Physik, Martin-Luther-Universität Halle-Wittenberg, D-06099 Halle, Germany*

(Received 19 December 2014; revised manuscript received 10 February 2015; published 27 February 2015)

Self-consistent *GW* calculations and the solution of the Bethe-Salpeter equation are to date the best available approaches to simulate electronic excitations in a vast class of materials, ranging from molecules to solids. However, up to now numerical instabilities made it impossible to use these techniques to calculate optical absorption spectra of the best-known thin-film absorbers for solar cells: $Cu(In,Ga)(S,Se)_2$ chalcopyrites and $Cu_2ZnSn(S,Se)_4$ kesterites/stannites. We show here how to solve this problem using a finite-difference method in k space to evaluate the otherwise diverging dipole matrix elements, obtaining an excellent agreement with experiments. Having established the validity of this approach, we use it then to calculate the optical response of the less studied, but promising, $Cu_2ZnGe(S,Se)_4$ compounds, opening the way to predictive calculations of still unknown materials.

DOI: 10.1103/PhysRevB.91.075134 PACS number(s): 78.20.−e, 78.20.Bh, 88.40.jn

I. INTRODUCTION

Photovoltaics represent one of the most important sustainable energy sources today, and are expected to play an essential role in the future evolution of the world's energy supply. The solar cell marketis still dominated by multicrystalline silicon, despite competition from thin-film solar cells made of CdTe and $Cu(In,Ga)Se_2$. In 2013, the total thin-film market share reached only 10%, to be compared with 18% in 2009 [1], and a further decline of the thin-film market in 2014 is foreseen. These numbers show the urgent need to find new materials and processes for thin-film photovoltaic energy conversion, respecting crucial constraints on the costs, low-energy processing, nontoxicity, and availability of the constituting elements. An imperative requirement for a thin-film absorber is an optimal overlap of its absorption spectrum with the emission spectrum of the sun. The ideal absorber should possess a band gap of 1.2 to 1.5 eV and display a strong absorption at the optical edge [2].

The best-known absorber material for thin-film photovoltaics is at present $CuIn_xGa_{1-x}Se_2$, with a record energy conversion efficiency of 21.7% [3]. Its band gap can be tuned continuously between 1.04 and 1.65 eV by varying the In/Ga ratio. [4] In order to further reduce the materials costs of thin-film solar cells, efforts are being made to replace $Cu(In,Ga)Se_2$ by an indium-free material with similar properties [5]. As the most representative example, thin-film solar cells with $Cu_2ZnSn(S,Se)_4$ as absorber material have already made their way into industry [6]. The record efficiency of this family of thin-film solar cells is presently 12.6% [7]. The optical band gap of $Cu_2ZnSn(S,Se)_4$ can also be tuned between 1.0 and 1.5 eV by varying the S/Se ratio. Another, less intensively studied, compound with a potentially suitable band gap is $Cu_2ZnGe(S,Se)_4$ [8,9]. Despite the fact that Ge is not cheaper than Ga or In, $Cu_2ZnGeSe_4$ is however an explored alternative to $Cu(In,Ga)(S,Se)_2$ due to the nontoxicity of Ge and its established use in electronics.

$Cu(In,Ga)Se_2$ and $Cu_2ZnSn(S,Se)_4$ compounds have been investigated intensively both experimentally and theoretically. There exist two almost isoenergetic crystal phases of these materials, namely, the kesterite and the stannite structures, which differ by the distribution of Cu and Zn atoms. Using neutron diffraction, Schorr clarified that the ground state is the kesterite crystal structure (in agreement with calculations) [10], and identified at the same time Cu on Zn and Zn on Cu antisites as the prevailing intrinsic defects [11]. These defects are indeed those that transform the kesterite into the stannite structure, and their low formation energies explain the coexistence of disordered mixed kesterite/stannite phases in experimental samples. The scattering of band gap values measured by different groups, and the lower photovoltaic efficiency of $Cu_2ZnSn(S,Se)_4$ cells with respect to $Cu(In,Ga)Se_2$ cells, are generally ascribed to the presence of minority phases and/or disorder [12]. Optical gaps and absorption spectra have been measured for some of the $Cu(In,Ga)Se_2$ [4], $Cu_2ZnSn(S,Se)_4$ [12,13], and $Cu_2ZnGe(S,Se)_4$ compounds [14,15].

This picture shows that Cu-based thin-film solar cells are still progressing; however, there is clearly a need to optimize existing or to search for novel absorbers for high-efficiency devices. However, synthesizing a new compound and measuring its optical absorption spectrum are complex tasks; for example, careful surface preparation is required in order to obtain a well-resolved optical absorption spectrum [4,13].

The search for novel absorbers for photovoltaics can be aided by the ability to calculate, from first principles, accurate optical properties for all possible composing elements, and more generally for any atomic arrangement, ranging from

*skoerbel@uni-muenster.de
†silvana.botti@uni-jena.de

molecules to low-dimensional nanostructures and solids. In the framework of many-body perturbation theory, the Green's-function-based self-consistent (sc) GW method, combined with the solution of the Bethe-Salpeter equation (BSE), is to date the most reliable and versatile approach to calculate optical response functions. Such *ab initio* calculations of optical spectra have been performed on a very high level of accuracy for many materials, and it is acknowledged that an excellent qualitative and quantitative agreement with experiment can be obtained with these methods both for solids [16–23] and finite nano-objects [24–28].

We can find several *ab initio* calculations on band gaps of $Cu(In,Ga)Se_2$ and related compounds in the literature: Chen *et al.* carried out an extensive computational study on the ground-state structure and stability of a large number of such compounds using density-functional theory (DFT) [8]. They estimated band gaps with an empirical extrapolation scheme, based on available experimental data. Zhang *et al.* conducted a similar study with a hybrid DFT functional in order to include Hartree-Fock exchange, and in addition obtained quasiparticle band gaps from many-body methods (GW@PBE+U) to identify trends in the band gaps with composition [29]. Botti and co-workers went a step further and accounted for the effects of self-consistency in the calculation of GW band structures of $Cu(In,Ga)Se_2$ and $Cu_2ZnSn(S,Se)_4$ compounds [30–32]. However, most of these works focus on the quasiparticle band gaps rather than the optical ones; in other words, excitonic effects are neglected. Although for the well-studied materials $Cu(In,Ga)(S,Se)_2$ and $Cu_2ZnSn(S,Se)_4$, there is experimental evidence that excitonic effects are small [33–36], this is not the case for simple silicon, whose oscillator strength near the absorption onset is strongly enhanced by excitonic effects [17], and in general, this cannot be safely assumed *a priori* for any given absorber material.

A few *ab initio* calculations of optical spectra of $Cu(In,Ga)(S,Se)_2$ and $Cu_2ZnSn(S,Se)_4$ have also been published [37,38]. These studies used either time-dependent DFT (TDDFT) with a hybrid functional [37], or the random-phase approximation (RPA) starting from GW band structures [38]. Unfortunately, it is well known that TDDFT, using a standard approximation for the time-dependent exchange-correlation functional, fails to correctly account for excitonic effects [20,39]. Using, for example, hybrid functionals, TDDFT allows for a partial inclusion of the electron-hole interaction also for solids [37,40], but the quasiparticle band gaps are usually too small [41], and excitonic peaks remain generally underestimated. The general accuracy of TDDFT with hybrid functionals for optical spectra of bulk crystals is therefore not yet sufficiently established, so that the scGW + BSE approach is preferable. It has not been applied to this class of materials yet, a gap which we fill with the present work. More specifically, we chose to use the self-consistent Coulomb hole plus screened exchange approximation, followed by a GW one-shot calculation (G_0W_0@scCOHSEX), as we explain in Sec. II.

If one tries to calculate the optical absorption of bulk chalcopyrite $Cu(Ga,In)Se_2$, using standard implementations [42,43] of the scGW + BSE approach, the result is very deceiving. These compounds are in fact computationally challenging due to the presence of hybridized p-d states close to the top of the valence band, which are responsible for the closing of the Kohn-Sham gap in standard DFT calculations. In the long-wavelength limit, a vanishing Kohn-Sham band gap causes divergencies in the dipole transition matrix elements that are used to build up the response function in an RPA, TDDFT, or BSE calculation. In the standard implementations for the calculation of optical absorption, this remains true even when the eigenenergies are properly replaced by hybrid functional or GW quasiparticle energies, making the whole spectrum *collapse* into an enormous unphysical peak at the absorption edge.

In this article, we propose a general and computationally efficient solution to this problem, and present as a first application the calculation of the optical spectra of Cu-based chalcogenides.

This paper is organized as follows. In Sec. II we describe the many-body perturbation theory methods that we use, and we explain how we solve the numerical problems that arise when the starting DFT Kohn-Sham band gap is closed. Then, in Sec. III, we present the calculated imaginary part of the frequency-dependent dielectric permittivity, $\mathrm{Im}\{\epsilon_M\}$, for $Cu(In,Ga)Se_2$, $Cu_2ZnSn(S,Se)_4$, and $Cu_2ZnGe(S,Se)_4$ compounds, considering both kesterite and stannite crystal structures for $Cu_2ZnSn(S,Se)_4$. We discuss the level of agreement between calculation and available experimental data in Sec. IV, and close in Sec. V with a summary and further perspectives.

II. COMPUTATIONAL METHODS

A. DFT and scGW calculations

The chalcopyrite crystal structure of $Cu(In,Ga)(S,Se)_2$ compounds is derived from the zinc blende structure of ZnS by replacing half the Zn atoms with Cu and the other half with In (or Ga) atoms, in such a way that every cation has four S (or analogously Se) neighbors and each anion has two Cu and two In (or Ga) neighbors. To obtain the conventional unit cell of $Cu(In,Ga)(S,Se)_2$, the face-centered cubic conventional unit cell of zinc blende is doubled along c, the c/a ratio deviates slightly from 2, and the internal coordinate u of S or Se deviates slightly from $u = 1/4$. For example, in $CuInS_2$, S is at $(u,u,1/8)$ with $0.20 < u < 0.23$ [44]. To obtain a quaternary $Cu_2ZnSn(S,Se)_4$ crystal with kesterite or stannite symmetry, the two In (or Ga) atoms in the unit cell are further replaced by one Zn and one Sn atom (see Fig. 1). In a similar way, $Cu_2ZnGe(S,Se)_4$ is obtained from $Cu(In,Ga)(S,Se)_2$ by replacing two In or Ga atoms with one Zn and one Ge atom. For $Cu_2ZnSn(S,Se)_4$, we take into account both kesterite and stannite structures. For $Cu_2ZnGe(S,Se)_4$, we assume the kesterite structure, which is the theoretical ground-state structure, according to calculations in Ref. [8].

For all crystal structures, first a DFT calculation for the ground state is performed using the local-density approximation (LDA) in the parametrization of Perdew and Wang [45] of the data of Ceperly and Alder [46] for the exchange-correlation energy. We note that a different choice of semilocal density functional as a starting point, such as the generalized-gradient approximation of Perdew, Burke, and Ernzerhof [47], does not significantly open the Kohn-Sham band gap, which is either

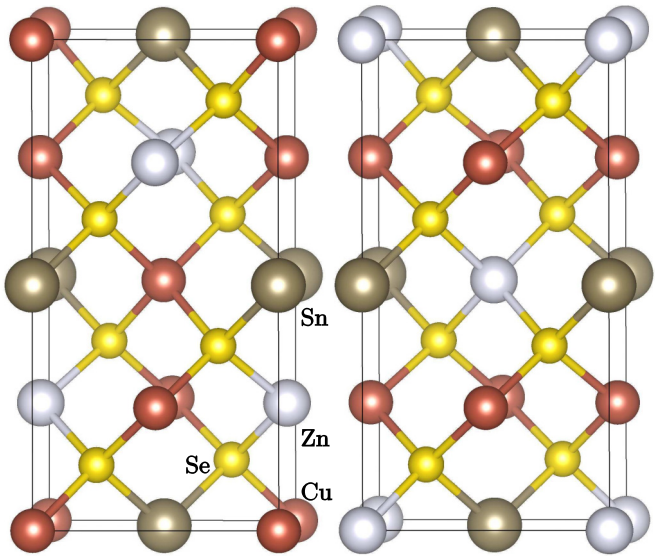

FIG. 1. (Color online) Crystal structures of $Cu_2ZnSnSe_4$ kesterite (left) and stannite (right), after Ref. [11].

negative or very small for all the compounds studied here. The experimental geometries [48–50] are used. When internal structural parameters are missing, they are calculated using the functional of Heyd, Scuseria, and Ernzerhof [51]. More details have been given in Refs. [30,32].

Afterwards, the many-body wave functions and energies are obtained with the GW method at the self-consistent COHSEX level [52]. The energy eigenvalues are further corrected by a perturbative GW (G_0W_0) calculation, using a plasmon-pole model [53] for the frequency dependence of the dielectric matrix. We note that this procedure allows photoemission band gaps in excellent agreement with experimental data to be obtained [30–32]. In Ref. [54], this G_0W_0@scCOHSEX approach has been compared to results of the LDA, the G_0W_0@LDA, and the quasiparticle self-consistent GW (QPscGW) method [55], which is self-consistent on energy eigenvalues and wave functions and delivers band gaps in excellent agreement with experiment [56]. Bruneval *et al.* conclude that G_0W_0@scCOHSEX improves strongly over LDA and G_0W_0@LDA and yields similar energy eigenvalues and electronic densities as QPscGW, at a lower computational cost. Throughout this paper, we apply this G_0W_0@scCOHSEX approach [54], which we call scGW. Monkhorst-Pack k-point meshes between $8 \times 8 \times 8$ and $16 \times 16 \times 16$ points, a plane-wave energy cutoff of 120 hartrees, and norm-conserving pseudopotentials are used. For Cu, In, Zn, and Sn, semicore states are included in the valence to properly account for the core-valence exchange interaction in the calculation of the self-energy [57–59], while 64 to 97 bands (about as many conduction as valence bands) are included. The scGW calculations are performed on a coarser k-point mesh ($3 \times 3 \times 3$ or $4 \times 4 \times 4$), in order to reduce the computational costs, and the quasiparticle energies are interpolated to finer k grids using maximally localized Wannier functions (MLWFs) [60–63]. All these calculations are performed with ABINIT [64,65]. All 64 to 97 bands are retained in the self-consistent COHSEX iterations, except for the lowest 8 to 20, depending on the system. For the calculation of the electronic screening, the energy cutoff is set to 50 hartrees for the plane-wave expansion of the wave functions, and to 15 hartrees for the size of the dielectric matrix. We note that only 240 to 300 bands are used thanks to the use of the extrapolar approximation of Bruneval and Gonze [66]. For the calculation of the self-energy, an energy cutoff of 70 hartrees is used for the plane-wave expansion of the wave functions and for the exchange self-energy, while a smaller matrix is needed for the correlation part of the self-energy, corresponding to a cutoff of 15 hartrees, consistent with the choice made for the dielectric matrix. In the final perturbative GW step, the convergence of the GW corrections with the number of included unoccupied states is again accelerated using the extrapolar approximation of Bruneval and Gonze [66]. All details on GW calculations for these systems can be found in previous publications [30–32].

B. Optical spectra

Optical spectra can be extracted from the frequency dependence of the imaginary part of the dielectric permittivity, $\mathrm{Im}\{\epsilon_M(\omega)\}$. Here we perform calculations of this tensor within the scGW RPA and by solving the BSE [67]. In order to compare with optical absorption experiments, we need the Fourier-transformed macroscopic dielectric permittivity in the long-wavelength limit [20],

$$\lim_{\mathbf{q}\to\mathbf{0}} \epsilon_M(\mathbf{q},\omega) = \lim_{\mathbf{q}\to\mathbf{0}} \frac{1}{\epsilon^{-1}_{\mathbf{G}=\mathbf{0},\mathbf{G}'=\mathbf{0}}(\mathbf{q},\omega)}, \tag{1}$$

where $\mathbf{q}$ is a wave vector in the first Brillouin zone. In the longitudinal gauge (which in the limit $\mathbf{q} \to \mathbf{0}$ becomes equivalent to the transverse one, with which we work), $\mathbf{q}$ is also parallel to the polarization of the light.

1. Optical spectra in the scGW RPA

The frequency-dependent dielectric permittivity in reciprocal space, $\epsilon_{\mathbf{G}\mathbf{G}'}(\mathbf{q},\omega)$, is connected to the linear density response function [20] $\chi(\mathbf{r},\mathbf{r}',t-t') = \delta\varrho(\mathbf{r},t)/\delta V_{\mathrm{ext}}(\mathbf{r}',t')$ as [42]

$$\epsilon^{-1}_{\mathbf{G}\mathbf{G}'}(\mathbf{q},\omega) = \delta_{\mathbf{G}\mathbf{G}'} + v_{\mathbf{G}}(\mathbf{q})\chi_{\mathbf{G}\mathbf{G}'}(\mathbf{q},\omega), \tag{2}$$

where ϱ is the electronic density, v is the Coulomb interaction, and χ can be obtained in the random phase approximation from the independent-particle response function $\chi^0(\mathbf{r},\mathbf{r}',t-t')$ from a Dyson equation, which we write using Fourier transforms in reciprocal and frequency space [42,59]:

$$\chi_{\mathbf{G}\mathbf{G}'}(\mathbf{q},\omega) = \chi^0_{\mathbf{G}\mathbf{G}'}(\mathbf{q},\omega) + \sum_{\mathbf{G}''} \chi^0_{\mathbf{G}\mathbf{G}''}(\mathbf{q},\omega)v_{\mathbf{G}''}(\mathbf{q})\chi_{\mathbf{G}''\mathbf{G}'}(\mathbf{q},\omega). \tag{3}$$

Note that in the RPA the Coulomb attraction between electron and hole is neglected.

The independent-particle response function χ^0 is often calculated using Kohn-Sham eigenvalues and orbitals [59]:

$$\chi^0{}_{\mathbf{G}\mathbf{G}'}(\mathbf{q},\omega) = \frac{1}{V}\sum_{\mathbf{k}nm} \frac{(f_{m\mathbf{k}+\mathbf{q}} - f_{n\mathbf{k}})\tilde{\varrho}_{nm\mathbf{k}}(\mathbf{q}+\mathbf{G})\tilde{\varrho}^*_{nm\mathbf{k}}(\mathbf{q}+\mathbf{G}')}{\omega - (E_{n\mathbf{k}} - E_{m\mathbf{k}+\mathbf{q}}) + i\eta\,\mathrm{sgn}(E_{n\mathbf{k}} - E_{m\mathbf{k}+\mathbf{q}})} \tag{4}$$

with the energy eigenvalues $E_{n\mathbf{k}}$, Fermi occupation numbers $f_{n\mathbf{k}}$, and oscillator matrix elements [59]

$$\tilde{\varrho}_{nm\mathbf{k}}(\mathbf{q}+\mathbf{G}) = \langle u_{n\mathbf{k}}|e^{-i(\mathbf{q}+\mathbf{G})\mathbf{r}}|u_{m\mathbf{k}+\mathbf{q}}\rangle, \tag{5}$$

where $u_{n\mathbf{k}}$ is the cell-periodic part of the Bloch function $\psi_{n\mathbf{k}}(\mathbf{r}) = \exp(i\mathbf{k}\cdot\mathbf{r})u_{n\mathbf{k}}(\mathbf{r})$. However, due to the mentioned shortcomings of Kohn-Sham DFT for the class of systems under study, in this work we will use the wave functions from scCOHSEX, and the energy eigenvalues from the quasiparticle results of the G_0W_0@scCOHSEX calculations described above (scGW RPA).

2. *Optical spectra in* scGW *BSE calculations*

So far, we have assumed electron and hole to be independent. This approximation is known to lead to poor absorption spectra for wide-gap semiconductors and silicon [20,39], and therefore we drop it here. First, in order to avoid the matrix inversion needed in Eq. (1), one writes [20,42]

$$\lim_{\mathbf{q}\to\mathbf{0}} \epsilon_M(\mathbf{q},\omega) = 1 - \lim_{\mathbf{q}\to\mathbf{0}} v_{\mathbf{G}=\mathbf{0}}(\mathbf{q})\bar{\chi}_{\mathbf{G}=\mathbf{0},\mathbf{G}'=\mathbf{0}}(\mathbf{q},\omega), \tag{6}$$

where the modified polarizability $\bar{\chi}$ is connected to χ^0 by [20]

$$\bar{\chi} = \chi^0 + \chi^0\bar{v}\bar{\chi}, \tag{7}$$

with the modified Coulomb potential [20]

$$\bar{v}_{\mathbf{G}}(\mathbf{q}) = \begin{cases} v_{\mathbf{G}}(\mathbf{q}) = 4\pi/(\mathbf{q}+\mathbf{G})^2 & \text{if} \quad \mathbf{G}\neq\mathbf{0}, \\ 0 & \text{if} \quad \mathbf{G}=\mathbf{0}. \end{cases} \tag{8}$$

Taking into account electron-hole interaction means including a vertex correction in Hedin's equation [52] for the polarizability. We define $L^0(1,2;3,4) = -iG(1,3)G(4,2)$, [20] the four-point polarizability for independent particles. Then, the modified four-point polarizability $\bar{L}$ is obtained from the Bethe-Salpeter equation [68]:

$$\bar{L} = L^0 + L^0\,\bar{\Xi}\,\bar{L}, \tag{9}$$

with the Bethe-Salpeter kernel $\bar{\Xi} = \bar{v} - W$ [68]. The RPA would be retrieved if W were set to 0. The four-point functions in Eq. (9) are expanded in a basis of products of quasiparticle conduction and valence states $\psi_{c\mathbf{k}}\psi^*_{v\mathbf{k}}$ [23]. In particular, L^0 is diagonal in this basis [23]:

$$L^0_{v_1,c_1,\mathbf{k}_1,v_2,c_2,\mathbf{k}_2}(\omega) = \frac{f_{c_1\mathbf{k}_1} - f_{v_1\mathbf{k}_1}}{E_{c_1\mathbf{k}_1} - E_{v_1\mathbf{k}_1} - \omega - i\eta}\delta_{v_1,v_2}\delta_{c_1,c_2}\delta_{\mathbf{k}_1,\mathbf{k}_2}. \tag{10}$$

Finally, the two-point polarizability $\bar{\chi}$ needed in Eq. (6) is a "diagonal" element of the four-point function $\bar{L}$: [20,59]

$$\bar{\chi}(1,2) = \bar{L}(1,2;1,2). \tag{11}$$

In order to avoid a time-consuming matrix inversion of Eq. (9), the BSE is solved using a series expansion [23]:

$$\bar{L} = (\mathbb{1} - L^0\bar{\Xi})^{-1}L^0 = \sum_m (L^0\bar{\Xi})^m L^0, \tag{12}$$

which is truncated at finite m once convergence is reached. The solution of the BSE is further sped up using a double-grid technique [23]. The quasiparticle energies from a scGW calculation are interpolated to a fine k grid (e.g., $24\times24\times24$ points) using maximally localized Wannier functions. The rapidly varying independent-particle polarization L^0 is calculated on this fine k grid, while the Bethe-Salpeter kernel $\bar{\Xi}$ is calculated on a coarser grid ($8\times8\times8$ or $10\times10\times10$ points). The mapping of L^0 to the coarser grid, on which the BSE is finally solved, is performed through the double-grid technique with a suitably chosen interpolation for the Bethe-Salpeter kernel (in this case with second-order polynomial interpolation). The fine k grid usually has three times more grid points in each direction compared to the coarse k grid, on which the spectra are obtained. A more detailed description of the double-grid technique can be found in Ref. [23].

3. *Dipole matrix elements*

Here we work in the length gauge, where the perturbation Hamiltonian due to the external electromagnetic field in the dipole approximation is $\mathbf{r}\cdot\mathbf{E}$, where $\mathbf{E}$ is the electric field. Alternatively, one could work in the velocity gauge, where the perturbation Hamiltonian would take the form $\mathbf{A}\cdot\mathbf{p}$, where $\mathbf{p}$ is the momentum operator, and $\mathbf{A}$ is the electromagnetic vector potential. Both for the scGW RPA and for the scGW BSE calculations, the oscillator matrix elements in Eq. (5) are needed. For $\mathbf{G}\neq\mathbf{0}$, $\tilde{\varrho}_{nm\mathbf{k}}(\mathbf{q}+\mathbf{G})$ can be obtained as a product in Fourier space. For the $\mathbf{G}=\mathbf{0}$ component of Eq. (5) in the limit $\mathbf{q}\to\mathbf{0}$,

$$\lim_{\mathbf{q}\to\mathbf{0}} \tilde{\varrho}_{nm\mathbf{k}}(\mathbf{q}) \approx -i \lim_{\mathbf{q}\to\mathbf{0}} \mathbf{q}\langle u_{n\mathbf{k}}|\mathbf{r}|u_{m\mathbf{k}}\rangle, \tag{13}$$

dipole matrix elements $\langle u_{n\mathbf{k}}|\mathbf{r}|u_{m\mathbf{k}}\rangle$ are usually first obtained in the basis of Kohn-Sham wave functions $|n\mathbf{k}^{\mathrm{KS}}\rangle$ and $|n'\mathbf{k}^{\mathrm{KS}}\rangle$, and then rotated into the basis of quasiparticle wave functions $|i\mathbf{k}\rangle$ and $|j\mathbf{k}\rangle$, as in Ref. [69]:

$$\langle i\mathbf{k}|\mathbf{r}|j\mathbf{k}\rangle = \sum_{n,n'} \langle i\mathbf{k}|n\mathbf{k}^{\mathrm{KS}}\rangle\langle n\mathbf{k}^{\mathrm{KS}}|\mathbf{r}|n'\mathbf{k}^{\mathrm{KS}}\rangle\langle n'\mathbf{k}^{\mathrm{KS}}|j\mathbf{k}\rangle. \tag{14}$$

The dipole matrix elements in the Kohn-Sham basis are typically evaluated as

$$\begin{aligned}\langle n\mathbf{k}^{\mathrm{KS}}|\mathbf{r}|n'\mathbf{k}^{\mathrm{KS}}\rangle &= \frac{\langle n\mathbf{k}^{\mathrm{KS}}|[\mathbf{r},\mathcal{H}^{\mathrm{KS}}]|n'\mathbf{k}^{\mathrm{KS}}\rangle}{E^{\mathrm{KS}}_{n'\mathbf{k}} - E^{\mathrm{KS}}_{n\mathbf{k}}} \\ &= \frac{\langle n\mathbf{k}^{\mathrm{KS}}|i\mathbf{p} + [\mathbf{r},V_{\mathrm{NL}}]|n'\mathbf{k}^{\mathrm{KS}}\rangle}{E^{\mathrm{KS}}_{n'\mathbf{k}} - E^{\mathrm{KS}}_{n\mathbf{k}}},\end{aligned} \tag{15}$$

where $E^{\mathrm{KS}}_{n\mathbf{k}}$ is a Kohn-Sham eigenvalue, and V_{NL} is the nonlocal part of the Kohn-Sham Hamiltonian due to nonlocal pseudopotentials. Because of the energy differences between Kohn-Sham states in the denominator, dipole matrix elements can be obtained from Eq. (15) only if DFT yields a finite band gap, so that $E^{\mathrm{KS}}_{n'\mathbf{k}} - E^{\mathrm{KS}}_{n\mathbf{k}} \neq 0$ [69]. In principle, Eq. (15) could be evaluated in the scGW basis, in which the band gap is finite. This, however, requires knowledge of the commutator of the position operator and the nonlocal part of the self-energy, $[\mathbf{r},\Sigma^{GW}_{\mathrm{NL}}]$, which is more difficult to obtain than its analog in the Kohn-Sham basis $[\mathbf{r},V_{\mathrm{NL}}]$. For the same reason, using hybrid functionals to open the band gap is not a simple solution. Therefore, we follow a different approach here: For transitions with a vanishing energy difference in DFT, we calculate the dipole matrix elements as k derivatives, based on the work by Blount [70]:

$$\langle v\mathbf{k}^{\mathrm{KS}}|\mathbf{r}|c\mathbf{k}^{\mathrm{KS}}\rangle = i\langle u^{\mathrm{KS}}_{v\mathbf{k}}|\nabla_{\mathbf{k}}|u^{\mathrm{KS}}_{c\mathbf{k}}\rangle, \tag{16}$$

using a finite-difference sum in k space,

$$\langle u_{v\mathbf{k}}^{\mathrm{KS}}|\nabla_{\mathbf{k}}|u_{c\mathbf{k}}^{\mathrm{KS}}\rangle \approx \sum_{\mathbf{b}} w_{\mathbf{b}}\mathbf{b}\langle u_{v\mathbf{k}}^{\mathrm{KS}}|u_{c\mathbf{k}+\mathbf{b}}^{\mathrm{KS}}\rangle, \tag{17}$$

where $\mathbf{b}$ is a vector to a (nearest-)neighbor k point, and the $w_{\mathbf{b}}$ are weight factors chosen such that the finite-difference sum is exact in the linear limit. This approach follows the work of Marzari and Vanderbilt discussed in Ref. [61], where the representation of the position operator as a k derivative and its approximation by a finite-difference sum are used in order to calculate and optimize the localization of Wannier functions. It is also related to the Berry-phase [71] approach to the electric polarization in solids [72]. In order to calculate the electric polarization of a periodic system in the Berry-phase approach, one needs the diagonal elements ($\langle v\mathbf{k}^{\mathrm{KS}}|\mathbf{r}|v\mathbf{k}^{\mathrm{KS}}\rangle$) in Eq. (16), which are not gauge covariant. However, here we are interested in the nondiagonal elements, assuming that band mixing by scGW in Eq. (14) is small. Under a gauge transformation, which multiplies the Bloch functions by an arbitrary phase factor for each band and k point,

$$|u_{n\mathbf{k}}^{\mathrm{KS}}\rangle \rightarrow |\tilde{u}_{n\mathbf{k}}^{\mathrm{KS}}\rangle = e^{i\varphi_{n\mathbf{k}}}|u_{n\mathbf{k}}^{\mathrm{KS}}\rangle, \tag{18}$$

the matrix elements $i\langle u_{v\mathbf{k}}^{\mathrm{KS}}|\nabla_{\mathbf{k}}|u_{c\mathbf{k}}^{\mathrm{KS}}\rangle$ transform in the same way as the position matrix elements [70]:

$$\begin{aligned}\langle u_{v\mathbf{k}}^{\mathrm{KS}}|\mathbf{r}|u_{c\mathbf{k}}^{\mathrm{KS}}\rangle &\rightarrow e^{i(\varphi_{c\mathbf{k}}-\varphi_{v\mathbf{k}})}\langle u_{v\mathbf{k}}^{\mathrm{KS}}|\mathbf{r}|u_{c\mathbf{k}}^{\mathrm{KS}}\rangle,\\ i\langle u_{v\mathbf{k}}^{\mathrm{KS}}|\nabla_{\mathbf{k}}|u_{c\mathbf{k}}^{\mathrm{KS}}\rangle &\rightarrow e^{i(\varphi_{c\mathbf{k}}-\varphi_{v\mathbf{k}})}i\langle u_{v\mathbf{k}}^{\mathrm{KS}}|\nabla_{\mathbf{k}}|u_{c\mathbf{k}}^{\mathrm{KS}}\rangle,\end{aligned} \tag{19}$$

whereas the matrix elements in Eq. (17) transform as

$$\langle u_{v\mathbf{k}}^{\mathrm{KS}}|u_{c\mathbf{k}+\mathbf{b}}^{\mathrm{KS}}\rangle \rightarrow e^{i(\varphi_{c\mathbf{k}}-\varphi_{v\mathbf{k}})}\langle u_{v\mathbf{k}}^{\mathrm{KS}}|u_{c\mathbf{k}+\mathbf{b}}^{\mathrm{KS}}\rangle e^{i(\varphi_{c\mathbf{k}+\mathbf{b}}-\varphi_{c\mathbf{k}})}.$$

Equation (17) is therefore not strictly gauge covariant, but it becomes asymptotically so in the limit of $\mathbf{b} \rightarrow \mathbf{0}$ for all gauges which are sufficiently smooth functions of $\mathbf{k}$. The phases can be chosen arbitrarily, apart from a constraint which results from the periodicity of the Bloch functions in k, $\psi_{n\mathbf{k}+\mathbf{G}} = \psi_{n\mathbf{k}}$ [72], which leads to

$$u_{n\mathbf{k}+\mathbf{G}}(\mathbf{G}') = u_{n\mathbf{k}}(\mathbf{G}'+\mathbf{G}). \tag{20}$$

In order to account for the possibility that a DFT program may output Bloch functions with random phases, for which Eq. (16) is undefined, we first switch to a gauge for which a derivative in k exists. A simple solution, which fulfills Eq. (20) and which we apply here, is a zero-order interpolation of the phases in each reciprocal lattice cell.

4. Technical details

Optical spectra are calculated using the program YAMBO [42]. Because of the optical anisotropy related to the symmetry of chalcopyrite (or kesterite and stannite), we consider light polarizations parallel and perpendicular to the crystallographic c axis. A Lorentzian smearing of 0.1 eV is applied to simulate thermal and other broadening present in experimental spectra. We include all bands used for the scCOHSEX calculations in the calculations using the scGW RPA, and about 20 bands (10 valence and 10 conduction bands) for the BSE calculations. For the BSE spectra, due to the small number of bands included, only an energy region of a few (about 4) eV can be covered. The scGW RPA spectra are found to be approximately converged with respect to the k-point density at about $8 \times 8 \times 8$ k points. We observe that the k-grid convergence is particularly critical for this class of materials as the lowest conduction band is very dispersive, and as a result, if we want to obtain a smooth first peak after the absorption threshold, a very dense sampling of the Brillouin zone around Γ is required. Furthermore, local-field effects are included, and the BSE coupling terms are omitted, i.e., we use the Tamm-Dancoff approximation (TDA). Finally, the static inverse dielectric matrix is calculated from the scCOHSEX wave functions and G_0W_0@scCOHSEX energy eigenvalues to build W for the BSE. In principle, one could apply the finite-difference approach throughout, but since its convergence with k points is slow (see below), we could not satisfactorily converge the matrix elements for large unit cells. Therefore we use a "mixed" approach, such that the commutator expression is used whenever possible. Only if the energy difference of a transition is smaller than a threshold, $|E_{n'\mathbf{k}}^{\mathrm{KS}} - E_{n\mathbf{k}}^{\mathrm{KS}}| < \delta$, is the matrix element calculated with the k derivative. In order to obtain a suitable value for δ, we first perform a scGW RPA calculation, using only k derivatives, on a finer k-point grid ($16 \times 16 \times 16$), in order to obtain the correct shape of the spectrum. Afterwards, another scGW RPA calculation is performed on a coarser k-point ($8 \times 8 \times 8$) grid with the mixed approach, choosing δ such that the onset of the spectrum on the coarse grid resembles that of the calculation on the finer grid (see Sec. III A). For the materials studied here, δ is of the order of 10^{-3}–10^{-2} hartrees. Finally, the BSE calculation is performed with the same δ. In the following, unless stated otherwise, the mixed approach is used throughout.

When comparing calculated with experimentally measured spectra, it is desirable to quantify the level of agreement in some way. It is straightforward to compare optical gaps, but for our purpose, the oscillator strength near the onset is also important. A criterion for "good" agreement between

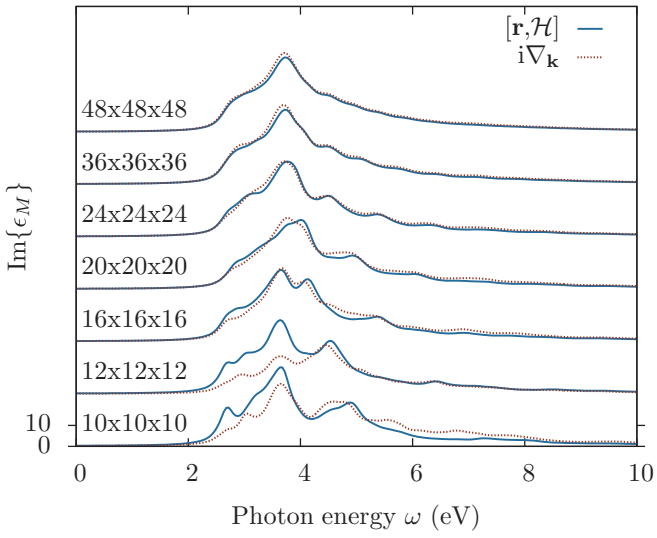

FIG. 2. (Color online) LDA RPA spectra of silicon using LDA wave functions and energies for k meshes from $10 \times 10 \times 10$ to $48 \times 48 \times 48$ points, calculated using the commutator expression $[\mathbf{r},\mathcal{H}]$, Eq. (15), and the k derivative $i\nabla_{\mathbf{k}}$, Eq. (16).

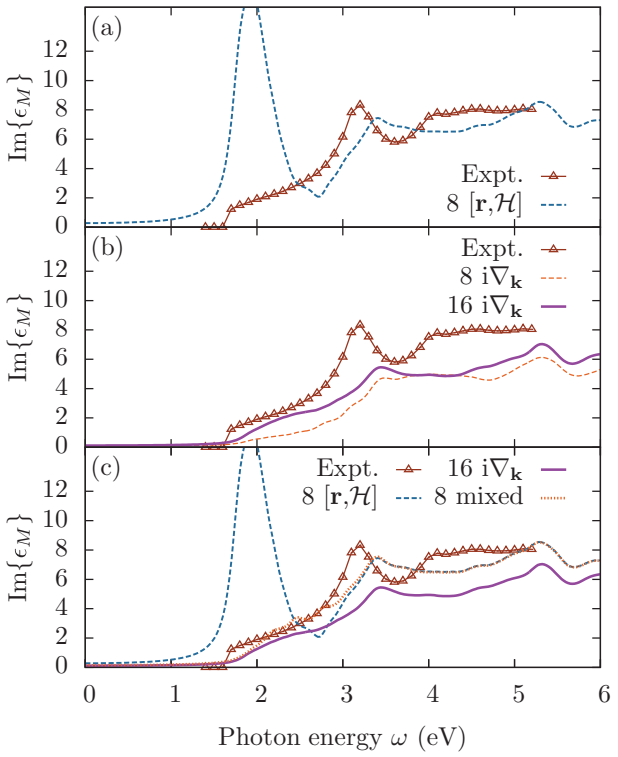

FIG. 3. (Color online) Imaginary part of ϵ_M of $CuGaSe_2$ from scGW RPA for light polarization || to the c axis, using (a) only the commutator expression; (b) only the k derivative; and (c), the combination of both (mixed, $\delta = 10$ millihartrees). The numbers 8 and 16 denote k-point meshes of $8 \times 8 \times 8$ and $16 \times 16 \times 16$ k points, respectively.

calculation and experiment could be, for example, that for a given set of materials, the calculated spectra can be assigned to the correct material and polarization direction by a numerical formula. In order to quantify the level of agreement between calculated and experimental spectra, we determine the overlap o_{ec} between normalized experimental (e) and calculated (c) spectra s as

$$o_{e\alpha,c\beta} = \frac{\langle s_{e\alpha} | s_{c\beta} \rangle}{\|s_{e\alpha}\| \|s_{c\beta}\|}, \tag{21}$$

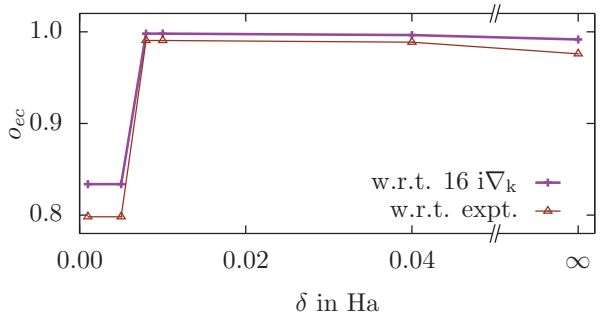

FIG. 4. (Color online) Overlaps of the normalized, mixed scGW RPA spectrum of $CuGaSe_2$ with the normalized $i\nabla_{\mathbf{k}}$ spectrum for $16 \times 16 \times 16$ k points and with the experimental one, as a function of δ for a k-point mesh of $8 \times 8 \times 8$ k points and for light polarization || to the c axis.

where the indices α and β denote light polarization directions perpendicular ($\perp$) and parallel (||) with respect to the crystallographic c axis, respectively. We test two criteria: (1) diagonal dominance of the overlap matrix, and (2) a positive determinant of the overlap matrix. The first criterion means that the calculated spectrum is more "similar" to the corresponding experimental one than to any other one. The second criterion is weaker; it means that the overall error is minimized if the spectra are correctly assigned. We normalize the determinant $d = \frac{\det o_{ec}}{\det o_{ee}}$ so that d ranges roughly from -1 (anticorrelation) to $+1$ (perfect correlation).

Optical gaps are extracted from a spectrum with a smaller broadening (1 meV) as the energy of the first local maximum (peak) of $\mathrm{Im}\{\epsilon_M(\omega)\}$ with a magnitude above 10^{-2}. The upper limit for the uncertainty in the peak position is 0.025 eV, the step between subsequent energies at which $\epsilon_M(\omega)$ is calculated.

III. RESULTS

A. Convergence tests for k derivatives

The finite-difference method, Eq. (17), requires a sufficiently high k-point density. In Fig. 2, the imaginary part of the frequency-dependent dielectric constant of silicon in the LDA RPA is depicted for different k-point meshes. Since the purpose is a convergence test with respect to k points, a correct band gap

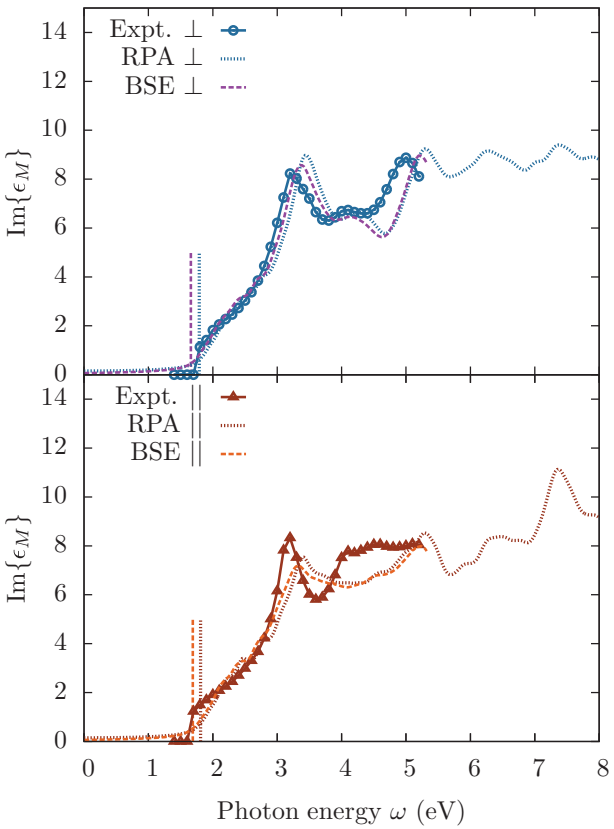

FIG. 5. (Color online) Imaginary part of ϵ_M of $CuGaSe_2$ from scGW RPA and scGW BSE calculations. A k mesh of $8 \times 8 \times 8$ points is used. Experimental data are from Alonso *et al.* [4]. The vertical lines indicate the calculated optical gaps using scGW RPA and scGW BSE (see Sec. III C).

is not important here, so that LDA wave functions and energy eigenvalues are used. The spectra obtained with k derivatives converge to those obtained with the commutator expression, but only for rather fine k-point grids of at least about $24 \times 24 \times 24$, whereas, at least for solving the BSE, we are limited to k-point grids of about $8 \times 8 \times 8$. Figure 3 shows the spectra of $CuGaSe_2$ from experiment [4] and calculated within the scGW RPA, using (a) only the commutator expression; (b) only the k derivative; and (c), the combination of both (mixed). The commutator expression leads to divergence of the first peak due to the underestimation of the band gap by DFT. The k derivative is free of such instabilities and yields a spectrum in qualitative agreement with experiment. However, since k-point convergence is not reached, the spectrum is too small, especially for the coarser k-point grid of $8 \times 8 \times 8$ points. At $16 \times 16 \times 16$ k points, the $i\nabla_{\mathbf{k}}$ spectrum is not yet converged with respect to k points, but comparing the upper, numerically stable part above 3 eV with the $[\mathbf{r},\mathcal{H}]$ spectrum, one notices that the shapes are already the same, and that lack of convergence of the $i\nabla_{\mathbf{k}}$ spectrum leads to a systematic underestimation of oscillator strength. By mixing the two methods, we take advantage of the numerical robustness of the k derivatives and the faster k-point convergence of the commutator expression. The spectrum is not a smooth function of δ. If δ is too small, divergent dipole matrix elements can occur. Once δ crosses a material-dependent threshold, the divergent matrix elements become finite abruptly. If δ is further increased, more $i\nabla_{\mathbf{k}}$ transitions are included, and the quality of the spectrum can decrease again, depending on the number of k points used. In Fig. 4 the experimental spectrum of $CuGaSe_2$ and the $i\nabla_{\mathbf{k}}$ spectrum for $16 \times 16 \times 16$ k points are used as a reference, and the normalized overlap with the calculated scGW RPA spectrum is depicted as a function of δ.

B. Spectra of $CuGaSe_2$, $CuInSe_2$, $Cu_2ZnSn(S,Se)_4$, and $Cu_2ZnGe(S,Se)_4$

Figure 5 shows the spectra of $CuGaSe_2$ from experiment [4] and calculated using the scGW RPA and the scGW BSE, using the mixed approach, as described above. The scGW RPA and scGW BSE methods yield very similar spectra, but the peak positions of the BSE spectra are shifted to slightly lower energies and are therefore in better agreement with experiment. A small difference between experimental and calculated peak positions, however, of about 0.1 to 0.2 eV remains, and the peak heights are apparently underestimated by the calculation in the region between about 4 and 5 eV (we discuss possible reasons below). The spectra of $CuInSe_2$ are depicted in Fig. 6. Already at the scGW RPA level, the agreement with experiment for the perpendicular polarization direction is excellent, apart from the first peak, which is much more pronounced in the calculated spectrum than in the experimental one. Note that if the LDA states are used in conjunction with a scissor operator to open the gap, spurious peaks appear in the onset region (not shown).

Figures 7 and 8 depict the spectra of the kesterite structure of Cu_2ZnSnS_4 and $Cu_2ZnSnSe_4$. In agreement with Refs. [38]

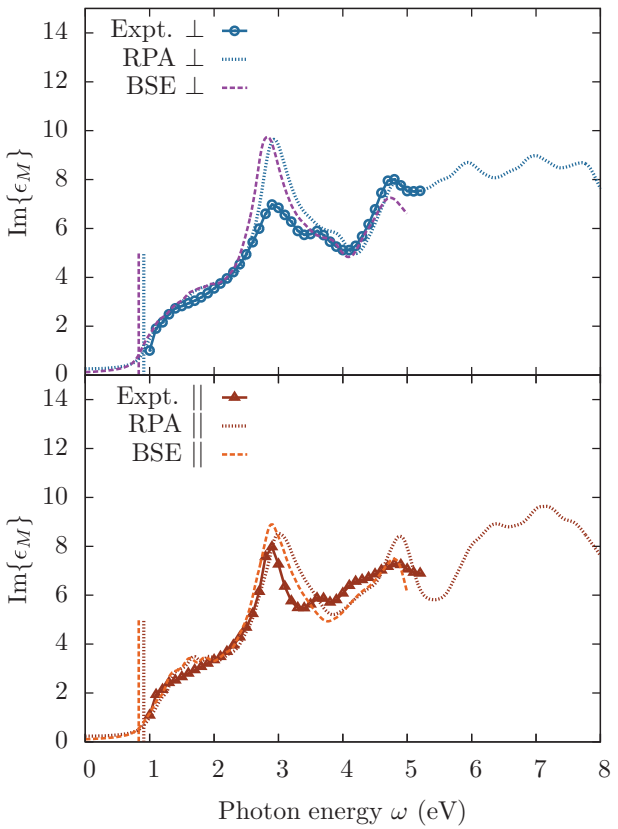

FIG. 6. (Color online) The same as Fig. 5 for $CuInSe_2$. A k mesh of $10 \times 10 \times 10$ points is used. Experimental data are from Alonso *et al.* [4].

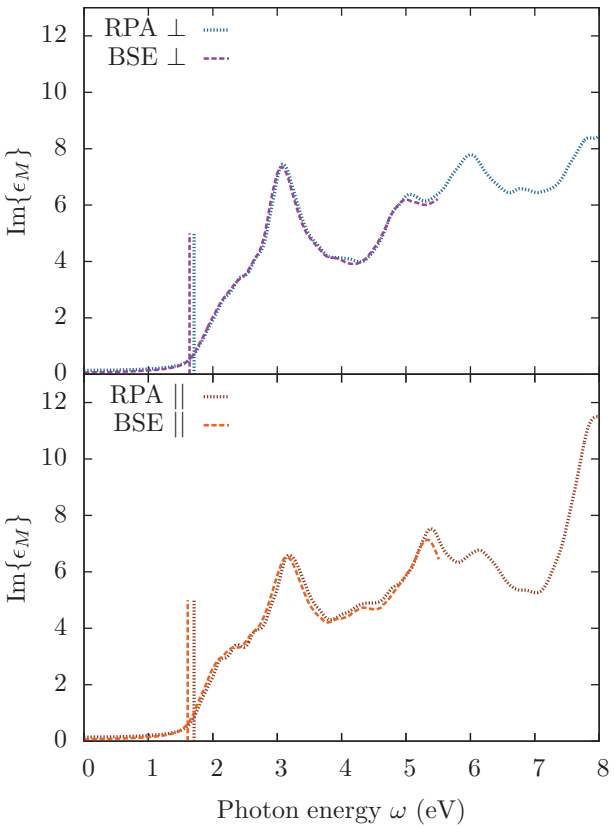

FIG. 7. (Color online) The same as Fig. 5 for Cu_2ZnSnS_4 kesterite.

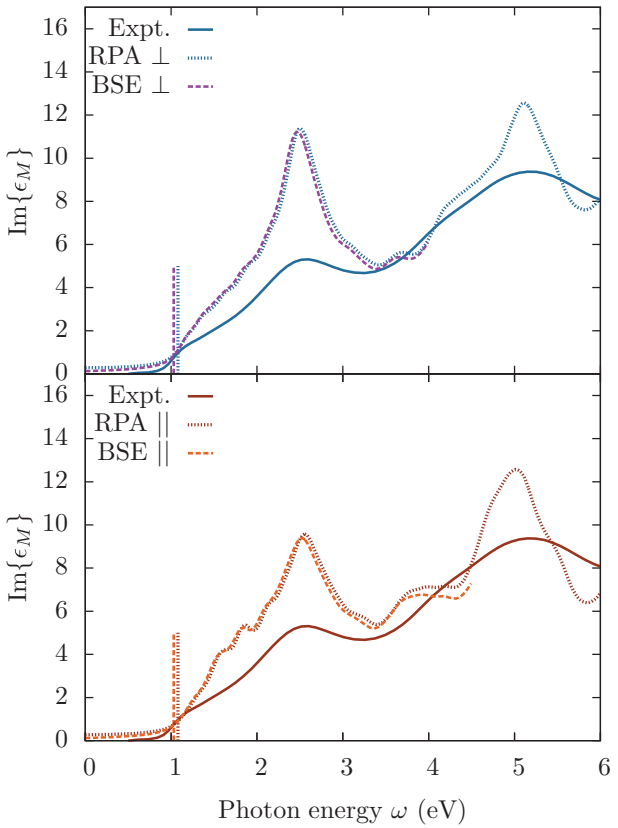

FIG. 8. (Color online) The same as Fig. 5 for $Cu_2ZnSnSe_4$ kesterite. Experimental data are from Choi *et al.* for an unknown polarization direction [13].

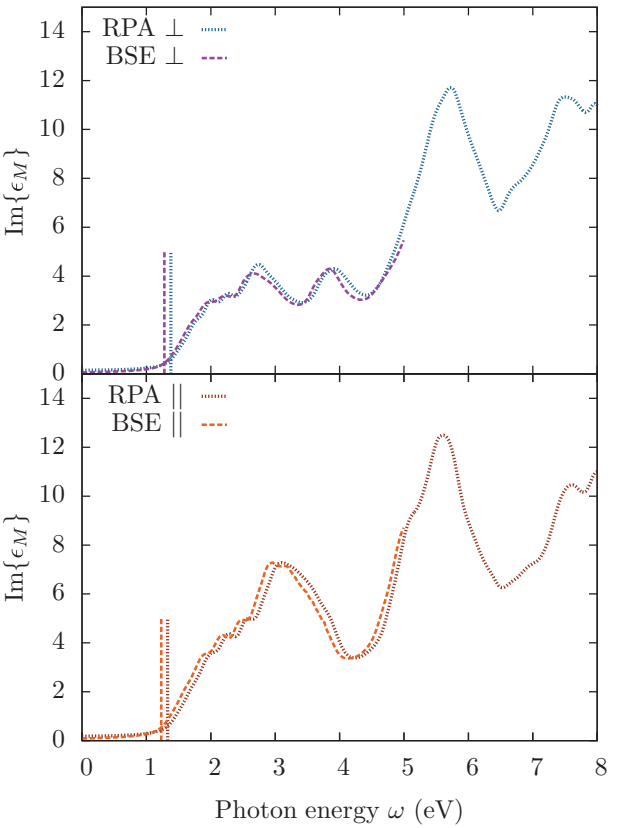

FIG. 9. (Color online) The same as Fig. 5 for Cu_2ZnSnS_4 stannite.

and [37], we obtain spectra that are nearly isotropic in the onset region. The onset of the spectrum is shifted to a lower energy if S is replaced by Se, in agreement with experiment. For the experimental spectrum of $Cu_2ZnSnSe_4$ kesterite, the polarization direction with respect to the c axis is not known. For both polarization directions, the calculated and experimental peak positions are compatible, due to the small anisotropy. The computed optical spectra of Cu_2ZnSnS_4 and $Cu_2ZnSnSe_4$ stannite are much more anisotropic than those of the other compounds studied here (see Figs. 9 and 10), in agreement with calculation results of Persson [38] and Paier [37]. For Cu_2ZnGeS_4 and $Cu_2ZnGeSe_4$, again almost isotropic spectra are obtained (see Figs. 11 and 12). As for $CuGaSe_2$, the peak positions calculated for Cu_2ZnGeS_4 are at slightly higher energies than the experimental ones. The BSE improves slightly over the RPA.

Using the criterion that the overlap matrix be diagonally dominant, the RPA can correctly assign the spectra to the right material, but fails to correctly distinguish between the polarization directions. Since the two materials are almost isotropic, this is not surprising. However, if we use the criterion of the determinant of the overlap matrix (see Table I), we obtain a positive normalized determinant $d = 0.50$ for $CuGaSe_2$and $d = 0.27$ for $CuInSe_2$, if we use the BSE (the RPA gives $d = 0.38$ and $d = -0.03$, respectively), which means that the BSE assigns the polarization directions correctly if the determinant is used for the distinction. Figure 13 shows the

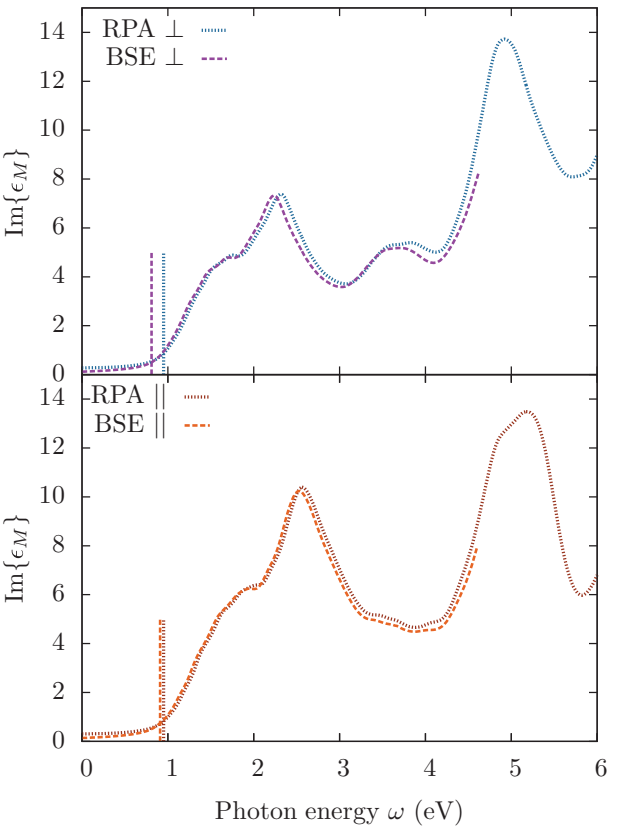

FIG. 10. (Color online) The same as Fig. 5 for $Cu_2ZnSnSe_4$ stannite. A k mesh of $10 \times 10 \times 10$ points is used.

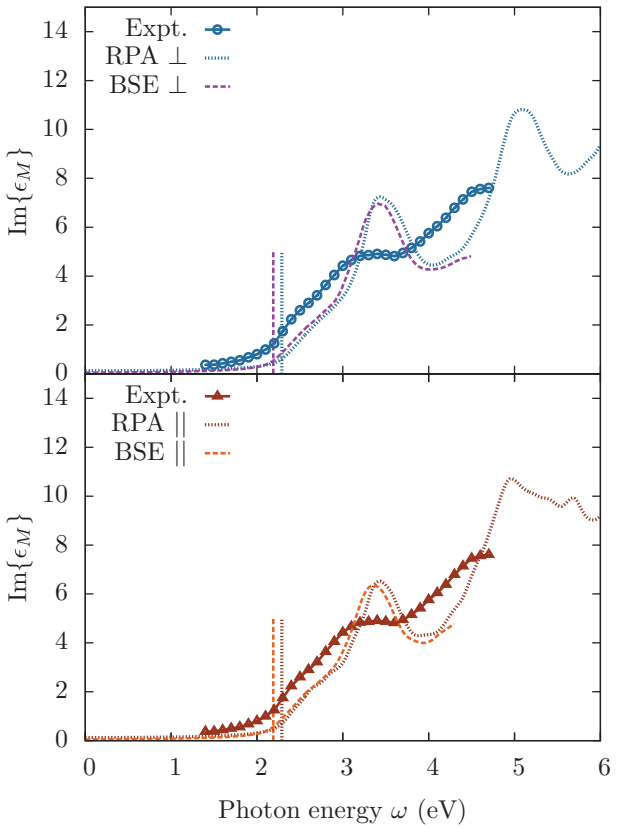

FIG. 11. (Color online) The same as Fig. 5 for Cu_2ZnGeS_4 kesterite. Experimental data are from León *et al.* [14] for the stannite structure for an unknown polarization direction.

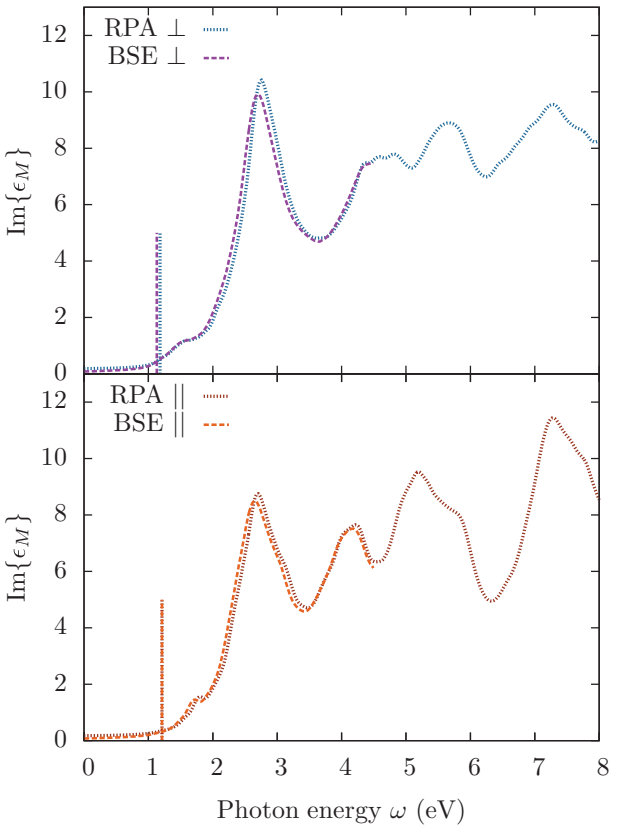

FIG. 12. (Color online) The same as Fig. 5 for $Cu_2ZnGeSe_4$ kesterite.

overlap matrix between the experimental and BSE spectra of $CuGaSe_2$ and $CuInSe_2$. The results for the RPA look very similar (not shown).

C. Optical gaps

Quasiparticle band gaps from scGW calculations at the Γ point, and optical gaps from the scGW RPA and from the scGW BSE, for light polarization directions perpendicular (⊥) and parallel (||) to the c axis, are presented for $CuGaSe_2$ (CGSe), $CuInSe_2$ (CISe), Cu_2ZnSnS_4 (CZTS), $Cu_2ZnSnSe_4$ (CZTSe), Cu_2ZnGeS_4 (CZGS), and $Cu_2ZnGeSe_4$ (CZGSe), for the kesterite (KES) and stannite (ST) structures of the quaternary compounds. The optical gaps are compiled in Table II and depicted in Fig. 14. The experimental gaps and those from scGW are not direction resolved. MAE stands for mean absolute error with respect to experiment. Experimental values are from Ref. [4] for $CuGaSe_2$ and $CuInSe_2$, from Refs. [12] and [32] and references therein for Cu_2ZnSnS_4 and $Cu_2ZnSnSe_4$, and from Ref. [15] for Cu_2ZnGeS_4 and $Cu_2ZnGeSe_4$. The MAE is below 0.2 eV for all three methods; it is smallest for scGW (0.1 eV).

IV. DISCUSSION

We observe the following: First, with our computational setup we obtain good overall agreement between calculated and experimental spectra. Second, this agreement is achieved already at the scGW RPA level, and the spectra obtained with the scGW BSE are very similar. In other words, for this family of compounds, excitonic effects on the spectra are small. Third, the scGW correction of the band structure and the wave functions yields better agreement with experiment than simply using a scissor operator (not shown). Fourth, the level of agreement with experiment is not uniform. For $CuGaSe_2$, $CuInSe_2$, and Cu_2ZnGeS_4, the peaks in the RPA spectra are shifted to higher energies compared to experiment. The shift is diminished, but not removed, by the use of the BSE in the TDA made here. In addition, the calculated oscillator strengths are smaller than the experimental ones in the region between about 4 and 5 eV for $CuGaSe_2$ and to some extent also for $CuInSe_2$, especially for light polarization parallel to the c axis. Although for molecules, carbon nanotubes, and organic semiconductors, the use of the TDA can affect the optical gap or peaks above the gap by up to several tenths of an eV [73–77], for inorganic semiconductors with a similar crystal structure to the ones studied here, namely, Si and GaAs, the TDA already yields an excellent agreement with experiment [17,19]. Therefore the use of the TDA is probably

TABLE I. Normalized determinant of the overlap matrix, as defined in Eq. (21).

Material	scGW RPA	scGW BSE
$CuGaSe_2$	0.38	0.50
$CuInSe_2$	−0.03	0.27

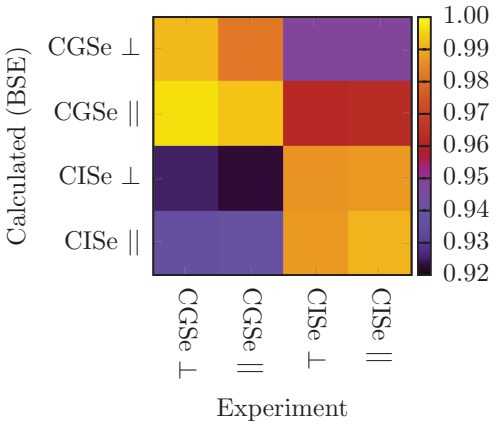

FIG. 13. (Color online) Overlap between experimental and scGW BSE spectra of $CuGaSe_2$ ("CGSe") and $CuInSe_2$ ("CISe").

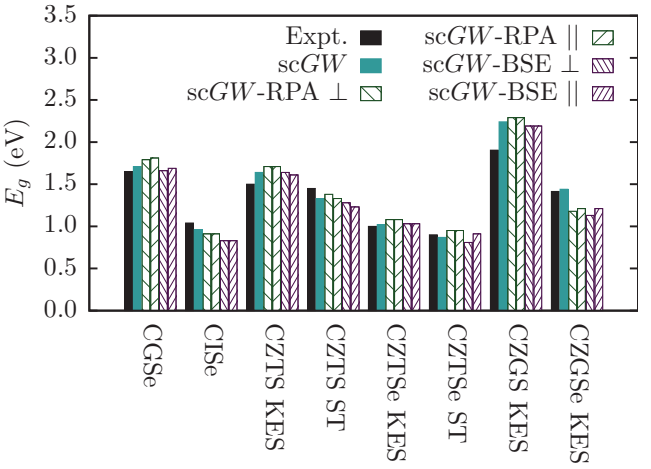

FIG. 14. (Color online) Optical band gaps from experiment, compared with the noninterpolated photoemission gaps calculated using the scGW method, and the optical gaps calculated using scGW-RPA and scGW-BSE, for $CuGaSe_2$ (CGSe), $CuInSe_2$ (CISe), Cu_2ZnSnS_4(S,Se) [CZTS, CZTSe], and Cu_2ZnGeS_4(S,Se) [CZGS, CZGSe] (see also Table II). KES and ST stand for kesterite and stannite structures, respectively.

appropriate here, and it is more likely that the observed discrepancies with respect to experiment arise already at the DFT or scGW level. The band-structure interpolation of the scGW energies from the coarse k grid used in the scGW calculations (usually $3 \times 3 \times 3$) may cause inaccuracies in the curvature of the bands, and therefore also in the width and position of spectral peaks. Finally, and perhaps most importantly, the band gaps of this type of compound, and probably also other parts of the band structure, depend very sensitively on the anion displacement parameter u [30,32,44], which is close to, but not equal to, 1/4 (in the parent structure ZnS it is exactly 1/4). $CuGaSe_2$, for which our calculated spectra are in less good agreement with experimental ones, is also the compound for which there is more uncertainty in the experimental u (it is either $u = 0.25$ or $u = 0.2431$), whereas the calculated one is $u = 0.264$ [44]. Here we have set $u = 0.25$, which may differ from the one in the sample for which the spectrum was recorded experimentally. Since the band gap depends very sensitively on u (in $CuInS_2$, the band gap changes by almost 2 eV if u changes from 0.20 to 0.25) [30], the same can be expected to be true for the position

TABLE II. Optical gaps from experiment, noninterpolated quasiparticle gaps from scGW calculations, and optical gaps from the scGW-RPA and from the scGW BSE (defined as the energy of the absorption onset; see Sec. II), for light polarization directions perpendicular ($\perp$) and parallel ($\|$) to the c axis.

	Expt.	scGW	scGW RPA		scGW BSE	
Material	$\perp$	$\|$	$\perp$	$\|$		
$CuGaSe_2$	1.65	1.71	1.79	1.81	1.66	1.69
$CuInSe_2$	1.04	0.96	0.91	0.91	0.83	0.83
Cu_2ZnSnS_4 KES	1.50	1.64	1.71	1.71	1.64	1.61
Cu_2ZnSnS_4 ST	1.45	1.33	1.38	1.33	1.28	1.23
$Cu_2ZnSnSe_4$ KES	1.00	1.02	1.08	1.08	1.03	1.03
$Cu_2ZnSnSe_4$ ST	0.90	0.87	0.95	0.95	0.81	0.91
Cu_2ZnGeS_4 KES	1.905	2.24	2.29	2.29	2.19	2.19
$Cu_2ZnGeSe_4$ KES	1.415	1.44	1.18	1.21	1.13	1.21
MAE		0.10	0.16	0.17	0.15	0.14

and strength of absorption peaks. Although we have used comparatively few (64) bands for $CuGaSe_2$, which may lead to underestimation of oscillator strength at higher transition energies (mainly above 4 to 5 eV), the spectrum onset is converged with respect to the number of included bands. We emphasize that the discrepancies with experiment discussed here are nevertheless quite small, compared to differences between experimental spectra measured by different groups on different samples [31]. The gaps obtained with scGW, scGW RPA, and scGW BSE are in excellent agreement with experiment (MAE below 0.2 eV). Although here the scGW method gives the smallest error (MAE of 0.1 eV), in cases where excitonic effects may be important, or where the lowest transitions may be dipole forbidden, optical gaps should be extracted from the scGW RPA or the scGW BSE instead. We notice that the Wannier interpolation of the scGW bands leads to a very small underestimation of the quasiparticle gap (not visible in the plotted spectra), compared to the interpolated one, which slightly affects the optical gaps on both the scGW RPA and the scGW BSE levels. As a consequence, and also due to the fact that exciton binding energies are negligible, the best agreement with experimental optical gaps is found for the noninterpolated scGW photoemission gaps. Since the exciton binding energies are tiny, the precision of our calculations does not allow us to determine them.

V. SUMMARY AND CONCLUSION

Optical spectra and optical gaps of $Cu(In,Ga)Se_2$, $Cu_2ZnSn(S,Se)_4$, and $Cu_2ZnGe(S,Se)_4$ have been calculated with *ab initio* many-body methods, namely, using the RPA and the BSE on top of the self-consistent COHSEX + G_0W_0 method, employing a numerically efficient double-grid technique. The level of agreement between calculation and experiment is better than 0.2 eV on average for the optical

gaps. In the materials studied here, excitonic effects are apparently very small, but in the cases of $CuGaSe_2$, $CuInSe_2$, and $Cu_2ZnSn(S,Se)_4$, they bring the positions of the main peaks into closer agreement with experiment. In this work, we have used a full state-of-the-art *ab initio* many-body methodology (self-consistent GW combined with the solution of the Bethe-Salpeter equation) for "pathological" materials, for which the calculation of optical spectra is difficult due to their vanishing Kohn-Sham band gap using a (semi)local exchange-correlation functional. This approach allows reproduction of experimental spectra up to subtle features such as the optical anisotropy of $CuGaSe_2$ and $CuInSe_2$. The remaining small differences between measured and calculated spectra are most likely related to differences in crystal structure between experiment and calculation. The approach taken here is free of empirical parameters, independent of the DFT functional used for the underlying ground-state calculation, and equally applicable to materials with weakly and strongly bound excitons. A further development of the method, which involves an interpolation of the k derivatives to accelerate k-point convergence, is currently under way. In this way, it may become possible to obtain optical spectra of problematic materials directly for moderately dense k-point meshes, instead of first performing a calculation on a finer k-point mesh, as was necessary for this work.

ACKNOWLEDGMENTS

We are grateful to Xavier Blase, Paul Boulanger, Matteo Gatti, and Lucia Reining for many fruitful discussions. We acknowledge support from the French Agence Nationale de la Recherche (ANR) (Grant No. ANR-12-BS04-0001-02). Computer time was granted by the French Grand Équipe National de Calcul Intensif (GENCI) (Project No. x2014096017).

[1] NPD solarbuzz PV equipment quarterly report, http://www.solarbuzz.com, 2013.
[2] M. Graetzel, R. A. Janssen, D. B. Mitzi, and E. H. Sargent, Nature (London) **488**, 304 (2012).
[3] Zentrum für Sonnenenergie und Wasserstoff-Forschung Baden-Württemberg (ZSW), press release, http://www.zsw-bw.de/uploads/media/pr12-2014-ZSW-WorldrecordCIGS.pdf, 2014.
[4] M. I. Alonso, K. Wakita, J. Pascual, M. Garriga, and N. Yamamoto, Phys. Rev. B **63**, 075203 (2001).
[5] H. Wang, Int. J. Photoenergy **2011**, 801292 (2011).
[6] T. K. Todorov, J. Tang, S. Bag, O. Gunawan, T. Gokmen, Y. Zhu, and D. B. Mitzi, Adv. Energy Mater. **3**, 34 (2013).
[7] W. Wang, M. T. Winkler, O. Gunawan, T. Gokmen, T. K. Todorov, Y. Zhu, and D. B. Mitzi, Adv. Energy Mater. **4**, 1301465 (2014).
[8] S. Chen, X. G. Gong, A. Walsh, and S.-H. Wei, Phys. Rev. B **79**, 165211 (2009).
[9] L. Shi, P. Yin, H. Zhu, and Q. Li, Langmuir **29**, 8713 (2013).
[10] S. Chen, X. G. Gong, A. Walsh, and S.-H. Wei, Appl. Phys. Lett. **94**, 041903 (2009).
[11] S. Schorr, Sol. Energy Mater. Sol. Cells **95**, 1482 (2011).
[12] S. Siebentritt and S. Schorr, Prog Photovoltaics: Research Applic. **20**, 512 (2012).
[13] S. Choi, H. Zhao, C. Persson, C. Perkins, A. Donohue, B. To, A. Norman, J. Li, and I. Repins, J. Appl. Phys. **111**, 033506 (2012).
[14] M. León, S. Levcenko, R. Serna, G. Gurieva, A. Nateprov, J. Merino, E. Friedrich, U. Fillat, S. Schorr, and E. Arushanov, J. Appl. Phys. **108**, 093502 (2010).
[15] D. B. Khadka and J. Kim, CrystEngComm **15**, 10500 (2013).
[16] L. X. Benedict, E. L. Shirley, and R. B. Bohn, Phys. Rev. Lett. **80**, 4514 (1998).
[17] S. Albrecht, L. Reining, R. Del Sole, and G. Onida, Phys. Rev. Lett. **80**, 4510 (1998).
[18] M. Rohlfing and S. G. Louie, Phys. Rev. Lett. **81**, 2312 (1998).
[19] M. Rohlfing and S. G. Louie, Phys. Rev. B **62**, 4927 (2000).
[20] G. Onida, L. Reining, and A. Rubio, Rev. Mod. Phys. **74**, 601 (2002).
[21] A. Marini and R. Del Sole, Phys. Rev. Lett. **91**, 176402 (2003).
[22] L. Chiodo, J. M. García-Lastra, A. Iacomino, S. Ossicini, J. Zhao, H. Petek, and A. Rubio, Phys. Rev. B **82**, 045207 (2010).
[23] D. Kammerlander, S. Botti, M. A. L. Marques, A. Marini, and C. Attaccalite, Phys. Rev. B **86**, 125203 (2012).
[24] M. Rohlfing and S. G. Louie, Phys. Rev. Lett. **80**, 3320 (1998).
[25] X. Blase and C. Attaccalite, Appl. Phys. Lett. **99**, 171909 (2011).
[26] L. Wirtz, A. Marini, and A. Rubio, Phys. Rev. Lett. **96**, 126104 (2006).
[27] M. Lopez del Puerto, M. L. Tiago, and J. R. Chelikowsky, Phys. Rev. Lett. **97**, 096401 (2006).
[28] M. Bruno, M. Palummo, A. Marini, R. Del Sole, and S. Ossicini, Phys. Rev. Lett. **98**, 036807 (2007).
[29] Y. Zhang, X. Sun, P. Zhang, X. Yuan, F. Huang, and W. Zhang, J. Appl. Phys. **111**, 063709 (2012).
[30] J. Vidal, S. Botti, P. Olsson, J.-F. Guillemoles, and L. Reining, Phys. Rev. Lett. **104**, 056401 (2010).
[31] I. Aguilera, J. Vidal, P. Wahnón, L. Reining, and S. Botti, Phys. Rev. B **84**, 085145 (2011).
[32] S. Botti, D. Kammerlander, and M. A. Marques, Appl. Phys. Lett. **98**, 241915 (2011).
[33] M. Yakushev, A. Mudryi, V. Gremenok, V. Zalesski, P. Romanov, Y. Feofanov, R. Martin, and R. Tomlinson, J. Phys. Chem. Solids **64**, 2005 (2003).
[34] F. Luckert, M. V. Yakushev, C. Faugeras, A. V. Karotki, A. V. Mudryi, and R. W. Martin, Appl. Phys. Lett. **97**, 162101 (2010).
[35] K. Hönes, E. Zscherpel, J. Scragg, and S. Siebentritt, Physica B **404**, 4949 (2009).
[36] F. Luckert, D. I. Hamilton, M. V. Yakushev, N. S. Beattie, G. Zoppi, M. Moynihan, I. Forbes, A. V. Karotki, A. V. Mudryi, M. Grossberg, J. Krustok, and R. W. Martin, Appl. Phys. Lett. **99**, 062104 (2011).
[37] J. Paier, R. Asahi, A. Nagoya, and G. Kresse, Phys. Rev. B **79**, 115126 (2009).
[38] C. Persson, J. Appl. Phys. **107**, 053710 (2010).
[39] S. Botti, A. Schindlmayr, R. Del Sole, and L. Reining, Rep. Prog. Phys. **70**, 357 (2007).
[40] J. Paier, M. Marsman, and G. Kresse, Phys. Rev. B **78**, 121201 (2008).

[41] M. A. L. Marques, J. Vidal, M. J. T. Oliveira, L. Reining, and S. Botti, Phys. Rev. B **83**, 035119 (2011).
[42] A. Marini, C. Hogan, M. Grüning, and D. Varsano, Comput. Phys. Commun. **180**, 1392 (2009).
[43] http://www.bethe-salpeter.org, 2014.
[44] J. E. Jaffe and A. Zunger, Phys. Rev. B **29**, 1882 (1984).
[45] J. P. Perdew and Y. Wang, Phys. Rev. B **45**, 13244 (1992).
[46] D. M. Ceperley and B. J. Alder, Phys. Rev. Lett. **45**, 566 (1980).
[47] J. P. Perdew, K. Burke, and M. Ernzerhof, Phys. Rev. Lett. **77**, 3865 (1996).
[48] H. W. Spiess, U. Haeberlen, G. Brandt, A. Räuber, and J. Schneider, Phys. Status Solidi B **62**, 183 (1974).
[49] S. R. Hall, J. T. Szymanski, and J. M. Stewart, Can. Mineral. **16**, 131 (1978).
[50] I. Olekseyuk, L. Gulay, I. Dydchak, L. Piskach, O. Parasyuk, and O. Marchuk, J. Alloys Compd. **340**, 141 (2002).
[51] J. Heyd, G. E. Scuseria, and M. Ernzerhof, J. Chem. Phys. **118**, 8207 (2003).
[52] L. Hedin, Phys. Rev. **139**, A796 (1965).
[53] R. W. Godby and R. J. Needs, Phys. Rev. Lett. **62**, 1169 (1989).
[54] F. Bruneval, N. Vast, and L. Reining, Phys. Rev. B **74**, 045102 (2006).
[55] S. V. Faleev, M. van Schilfgaarde, and T. Kotani, Phys. Rev. Lett. **93**, 126406 (2004).
[56] M. van Schilfgaarde, T. Kotani, and S. Faleev, Phys. Rev. Lett. **96**, 226402 (2006).
[57] M. Rohlfing, P. Krüger, and J. Pollmann, Phys. Rev. Lett. **75**, 3489 (1995).
[58] A. Marini, G. Onida, and R. Del Sole, Phys. Rev. Lett. **88**, 016403 (2001).
[59] F. Bruneval, Ph.D. thesis, Ecole Polytechnique, Palaiseau, 2005.
[60] A. A. Mostofi, J. R. Yates, Y.-S. Lee, I. Souza, D. Vanderbilt, and N. Marzari, Comput. Phys. Commun. **178**, 685 (2008).
[61] N. Marzari and D. Vanderbilt, Phys. Rev. B **56**, 12847 (1997).
[62] I. Souza, N. Marzari, and D. Vanderbilt, Phys. Rev. B **65**, 035109 (2001).
[63] D. R. Hamann and D. Vanderbilt, Phys. Rev. B **79**, 045109 (2009).
[64] X. Gonze, B. Amadon, P.-M. Anglade, J.-M. Beuken, F. Bottin, P. Boulanger, F. Bruneval, D. Caliste, R. Caracas, M. Cote, *et al.*, Comput. Phys. Commun. **180**, 2582 (2009).
[65] X. Gonze, Z. Kristallogr. **220**, 558 (2005).
[66] F. Bruneval and X. Gonze, Phys. Rev. B **78**, 085125 (2008).
[67] G. Strinati, Riv. Nuovo Cimento Soc. Ital. Fis. **11**, 1 (1988).
[68] F. Sottile, Ph.D. thesis, Ecole Polytechnique, Palaiseau, 2003.
[69] R. Asahi, W. Mannstadt, and A. J. Freeman, Phys. Rev. B **59**, 7486 (1999).
[70] E. Blount, Solid State Phys. **13**, 305 (1962).
[71] M. V. Berry, Proc. R. Soc. London, Ser. A **392**, 45 (1984).
[72] R. Resta, Rev. Mod. Phys. **66**, 899 (1994).
[73] Y. Ma, M. Rohlfing, and C. Molteni, Phys. Rev. B **80**, 241405 (2009).
[74] M. Grüning, A. Marini, and X. Gonze, Nano Lett. **9**, 2820 (2009).
[75] D. Rocca, D. Lu, and G. Galli, J. Chem. Phys. **133**, 164109 (2010).
[76] I. Duchemin, T. Deutsch, and X. Blase, Phys. Rev. Lett. **109**, 167801 (2012).
[77] P. Puschnig, C. Meisenbichler, and C. Draxl, arXiv:1306.3790.